Structure Analysis of the SECRAL Superconducting Magnet System*

HE Wei[1,2] ZHAO Hong-Wei[1;1)]

1 (Institute of Modern Physics (IMP), Chinese Academy of Sciences, Lanzhou 730000, China)
2 (Graduate University of Chinese Academy of Sciences, Beijing 100049, China)

Abstract An advanced superconducting ECR ion source named SECRAL has been constructed at Institute of Modern Physics of Chinese Academy of Sciences, whose superconducting magnet assembly consists of three axial solenoid coils and six sextupole coils with a cold iron structure as field booster and clamp. In order to investigate the structure of sextupole coils and to increase the structural reliabilities of the magnet system, global and local structural analysis have been performed in various operation scenarios. Winding pack and support structure design of magnet system, mechanical calculation and stress analysis are given in this paper. From the analysis results, it has been found that the magnet system is safe in the referential operation scenarios and the configuration of the magnet complies with design requirements of the SECRAL.

Key words superconducting magnet, ECR ion source

1 Introduction

In order to meet HIRFL-CSR and RIBLL's requirements for intense highly charged ion beams, the SECRAL ion source was designed and built at the Institute of Modern Physics (IMP). The SECRAL is a compact fully superconducting ECR ion source with an unique structure and high performance for intense heavy ion beams with very high charge states, such as 50—100eμA of Xe^{33+}, U^{41+} dc beam and 100—200eμA pulsed beam[1].

2 Overview of the superconducting magnet assembly of SECRAL

The SECRAL design has been optimized for maximum ion source performances at 28GHz RF frequency. The superconducting magnet assembly consists of three axial solenoid coils and six sextupole coils with a cold iron structure as field booster and clamp. At full excitation, this magnet assembly will produce peak mirror fields on axis of 3.6T at injection, 2.2T at extraction, and a radial sextupole field of 2.0T at plasma chamber wall. What is different from the traditional design, such as LBNL VENUS and LNS SERSE, is that the six sextupole coils are located outside of the three axial solenoids, which not only reduces the interaction forces between the sextupole and the solenoids but also enables the ion source much more compact, only 1m in length and 1m in diameter, which is very beneficial to RF coupling and beam extraction region. The sextupole magnet assembly consists of six segments with six racetrack superconducting coils. The superconducting coil of each sextupole segment is wound around one piece of iron pole as a sextupole field booster. Another iron

Received 20 April 2007
* Supported by Knowledge Innovation Program of Chinese Academy Sciences (KJCX1-09) and National Natural Foundation for Distinguished Young Scientist (10225523)
1) E-mail: zhaohw@impac.ac.cn

segment is fixed around the iron pole and the sextupole coil for the magnet clamping and field booster, which reduces the stray magnetic field coming out of the superconducting coils to a very low level less than 50Gs. This results in a very low interaction force between the magnet assembly and the iron yoke, which makes support of the magnet inside the cryostat much easier and is also good for the operation of the cryogenic cooler. The key feature for the SECRAL magnet clamping scheme is to utilize the magnetic forces experienced by the six sextupole segments and appropriate tolerances of the four aluminium shrinking rings, which make the magnet clamping much simple[1, 2]. The structure of the sextupole magnet assembly is shown in Fig. 1.

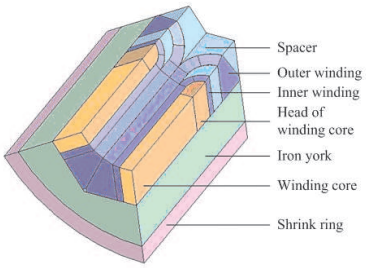

Fig. 1. The structure of the SECRAL 1/12th sextupole magnet assembly.

3 Finite element model and load case

The magnetic force distribution produced by the superconducting solenoid coils is so simple that it is easy to restrict. However, the magnetic force distribution produced by the superconducting sextupole coils is complicated, therefore we mainly simulated the mechanical behaviour of the sextupole assembly in this paper.

The geometry of the winding pack was predefined by physical demands. The contribution of several programs to get the results needed with the data mainstream used by the generation and optimization of the structural model is shown in a simplified flow diagram[3, 4] (Fig. 2).

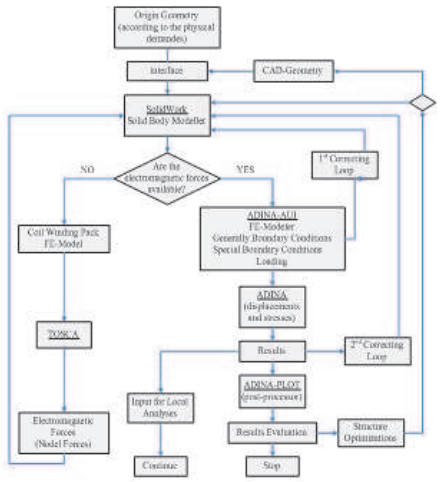

Fig. 2. Flow chart of program system used by the analysis of the structure.

A three-dimensional finite element (FE) model has been developed. The 1/12th sextupole magnet assembly is fully modelled with 27-node brick elements as shown in Fig. 3. The fact that the FE-model could be reduced to 1/12th is based on the special symmetry condition due to the coil geometry. These symmetry conditions allow on the other hand the derivation of specific boundary conditions. The symmetrical conditions inside of the coil system can be explained by means of Fig. 3. That implies the fact that there are two types of symmetric surfaces inside of the geometry which obey different symmetry conditions: the axial symmetry inside of winding pack which symmetry plane lie in the XY plane in the Fig. 3 and radial symmetry which symmetry axis is the Z axis in the Fig. 3. Assuming, the axial DOF (degree of freedom) in the axial symmetry plane is fixed and the azimuthal DOF in the radial symmetry plane is fixed. Additionally, the reduction of a FE-model in the way described above requires the following conditions:

- Both the CAD-model and FE-model have to obey the symmetry conditions described here
- The gravities must not to be taken into account in the analysis
- A case of disturbance can be analyzed conditionally only. The periodical disturbance can be taken into account

• This method might be used for the cases with small displacements only

Fig. 3. FE-model of the sextupole magnet structure.

Despite all these restrictions, with a 1/12th reduced model it is possible to analyze nearly all of the system relevant questions. A great advantage in the application of this method is the possibility of increased refinement of the element subdivision and this increases the accuracy of the computed results. Total number of elements and nodes are 4666 and 46171, respectively. The mechanical material properties used in the FE analysis are summarized in Tables 1∼2.

Table 1. Isotropic material properties in the FE-model.

material	temperature/K	Young's modulus/Pa	Poisson's ratio	thermal expansion ($\times10^{-6}$/K)
316L	293	2.0×10^{11}	0.3	10.3
	4	2.0×10^{11}	0.3	6.9
ARMCO	293	2.0×10^{11}	0.3	6.9
	4	2.0×10^{11}	0.3	6.9
Al	293	0.7×10^{11}	0.33	40.3
	4	0.8×10^{11}	0.33	40.3

Table 2. Anisotropic material properties in the FE-model.

material		wind		GRP	
temperature/K		193	4	293	4
Young's modulus	a	8.575	8.69	0.8	0.8
/($\times10^{10}$ Pa)	b	1.585	2.99	2.1	2.1
	c	1.585	2.99	2.1	2.1
shear moduli	ab	3.72	3.78	0.3	0.3
/($\times10^{10}$ Pa)	ac	0.61	1.02	0.3	0.3
	bc	0.61	1.2	0.8	0.8
Poisson's ratio	ab	0.15	0.15	0.12	0.12
	ac	0.25	0.25	0.12	0.12
	bc	0.3	0.3	0.32	0.32
thermal expansion	a	0.939	0.939	1.53	1.53
/($\times10^{-6}$/K)	b	1.39	1.39	0.686	0.686
	c	1.39	1.39	0.686	0.686

Note: a∼ Radial, b∼ Lateral, c∼ Circumferential.

The major loads acting on the sextupole assembly are dead load, assembling preload, thermal load due to cool down, and electromagnetic loads during operation, which are activated in time sequence. The criterion of the chosen load case as representative for the design analysis was the maximal current in sextupole coils. The related field value at 65mm radial is 2.0T. The forces exerted by the magnetic fields are determined by means of the TOSCA code based on the Biot–Savart law:

$$\boldsymbol{f} = \boldsymbol{j} \times \boldsymbol{B} \ .$$

Where is $\boldsymbol{f}$ the magnetic force density vector, $\boldsymbol{j}$ the current density vector and $\boldsymbol{B}$ the magnetic flux density vector. The force distribution within the coil is inhomogeneous. The values of the magnetic force density vary over the coil cross-section. The volume integral of the magnetic force densities results in a net force on each coil. For entire sextupole coils, the net vertical forces vanish due to the symmetry conditions of the coil system. The net coil forces are shown in Table 3. The magnetic force density distribution inside of the winding pack calculated by the TOSCA code has to be transformed into nodal forces used by the finite element analysis.

Except the material nonlinearities described above, the actual model considers the geometrical nonlinearities to define the contact surfaces between the particular parts of the FE-model described in fellow:

- Winding core and winding
- Winding core and iron yoke
- Inner winding and outer winding
- Winding and iron yoke
- Iron yoke and shrink ring

Those particular parts described above are laterally fixed at sides. This fixation is realized using the contact surface capability so that radial displacement (viewed in local coordinate system of the coil) is performed without constraints.

Table 3. The net forces in sextupole winding pack.

	F_x/N	F_y/N	F_r/N	θ	F_z/N
sextupole coil 1	2773877	-7996	2773889	0°	62197
sextupole coil 2	1380013	2406246	2773889	60°	-62197
sextupole coil 3	-1393864	2398250	2773889	120°	62197
sextupole coil 4	-2773877	7996	2773889	180°	-62197
sextupole coil 5	-1380013	-2406246	2773889	240°	62197
sextupole coil 6	1393864	-2398250	2773889	300°	-62197
resultant force of all sextupole coils	0	0			0

4 Analysis results

The finite element analysis by the ADINA code was performed. The model calculates displacements, forces and 3-D stress field in the sextupole assembly. The general conditions and assumption used for the analysis have to be taken into account during the evaluation of the results. These conditions and assumption are:

- The structure is loaded by static loads only
- Especially boundary conditions have been used by the model preparation
- The friction between the contact surfaces has been neglected

In the result band plots, the unit of displacement and stress is in mm and MPa, respectively. The effective stress is Von Mises stress. Stress-AA, BB and CC are the component stress in local coordinate system.

4.1 Displacements

Under all loads described above and defined boundary conditions, the displacements of winding core and winding are shown Figs. 4—7. Fig. 4 shows that contraction in the head of winding core is more than that in the middle of winding core along the radial direction, which seems the head of winding core to separate from the iron yoke. From Figs. 6—7, we can observe that contraction of winding along the axial direction is larger than that along the radial direction. From Figs. 4 & 6, Contraction in winding core is comparable with that in winding along the radial direction. However, From Figs. 5 & 7, contraction in the head of winding is larger than that in winding core along the axial direction, which indicates that the stress in the head of winding must be much larger.

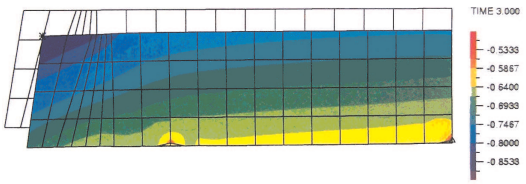

Fig. 4. Displacement of winding core along the radial direction.

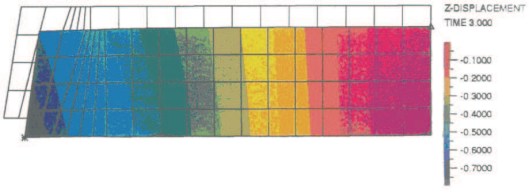

Fig. 5. Displacement of winding core along the axial direction.

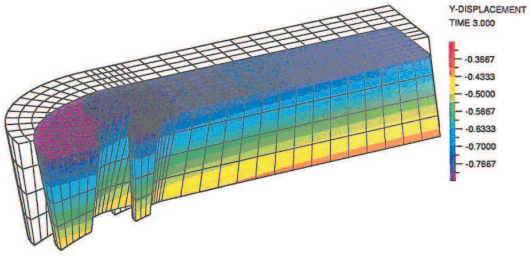

Fig. 6. Displacement of winding along the radial direction.

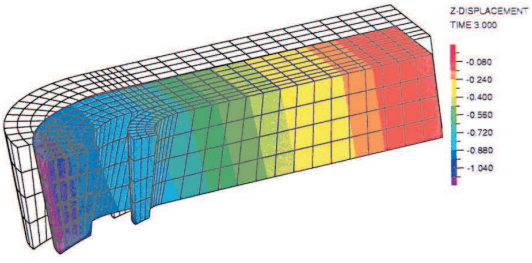

Fig. 7. Displacement of windings along the axial direction.

4.2 Stresses

Since the shrink ring and winding core will be made of stainless steel and soft iron with isotropic properties, respectively. It is sufficient to consider

the results of the effective stress (Von Mises). Due to the orthotropic material properties of the winding pack and spacer, some cares have to be taken for the result evaluation which is based on the local stress tensor. The critical point by the design of winding pack is the insulation shear stress. In this context, vacuum impregnated glass-fibre-reinforced epoxy insulation will be considered only. The value of 300MPa was given as acceptable for the operating conditions by the ACCEL Company. Additionally, a maximum strain limit of about 0.8% must not be exceeded in the superconducting cable because of the loss of the superconductivity.

The effective stress distribution in the winding core is shown in Fig. 8. It is indicated that the effective stresses are larger and the average is about 120MPa in the contact region between the head of winding core and iron yoke. Local compressive stress is exceed 150MPa nearby the inner radial surface of winding core, which results in torsion towards inside at the head of winding core. As a result, it is necessary to reduce these stresses by bolting the head of winding core.

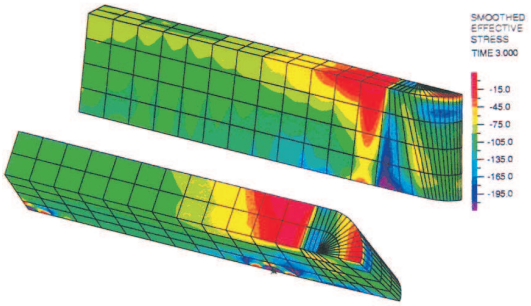

Fig. 8. Effective stress in winding core.

The stress distribution of the winding is computed in the local coordinates along current direction. In the follow result band plots, Stress-AA denotes axial stress in straight segment of winding (azimuth stress in the head of winding). Stress-BB refers to radial stress and Stress-CC indicates azimuth stress in straight segment of winding (axial stress in the head of winding).

The fact that the axial stress is approximate to 50—100MPa in straight segment of winding and the azimuth stress is less than 200MPa in the head of winding is shown in Fig. 9. Fig. 10 shows that azimuth stress is about −5MPa in straight segment of winding, which is the force compressing to the winding core. However, local regions nearby the head of winding are out of contact with winding core due to free-contact stress indicated in Fig. 11. The axial stress is much larger, more than about −80MPa in the head of winding.

The radial stress distribution is shown in Fig. 12, which is less than about 60MPa representing contract stress towards inner. Due to bending tensile stress appears in some local regions at the head of winding.

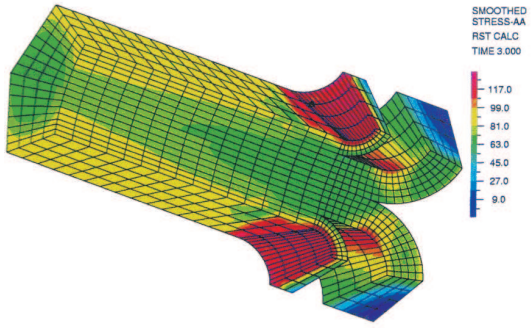

Fig. 9. Axial stress in straight segment of winding (the azimuth stress in the head of winding).

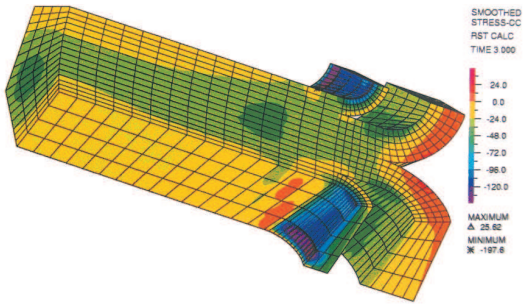

Fig. 10. Azimuthal stress in the straight segment of windings (the axial stress in the head of windings.

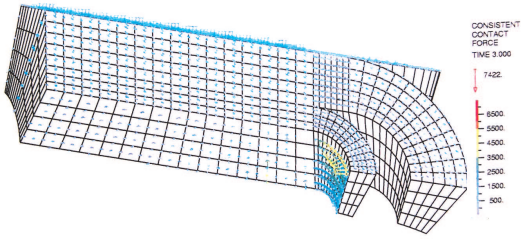

Fig. 11. The contact force in winding.

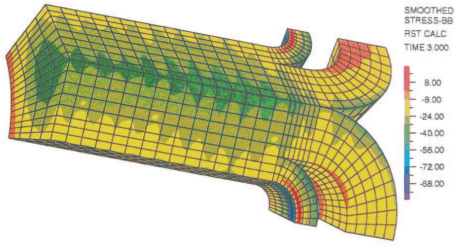

Fig. 12. The radial stress in winding.

5 Conclusion

To investigate the structural integrities and to increase the structural reliabilities of the sextupole magnet assembly, the structural analysis of sextupole magnet system has been performed for various analyzes such as a global/local analysis. From the analysis results, it has been found that the maximum stress intensities of the sextupole magnet structure are below the allowable stress limit, so it can safely withstand the reference operation scenarios and the structural integrity of the sextupole magnet complies with requirements of the design criteria for SECRAL magnet system.

References

1 ZHAO H W, SUN L T et al. Rev. Sci. Instrum., 2006, **77**: 03A333

2 ZHAO H W, ZHANG Z M et al. Rev. Sci. Instrum., 2004, **75**: 1410—1413

3 ADINA R&D Inc. A Finite Element Computer Program for Automatic Dynamic in Cremental Nonlinear Analysis System 7.5, 71 Elton Avenue, Watertown, MA 02472 USA, 2001

4 Bathe K J. Finite Element Procedures. Englewood Cliffs, NJ: Prentice-Hall, 1996